

Average Current Monitor Calibration

*

J. Welch

January 18, 2023

Contents

1	Introduction	1	6	Calibration functions	14
1.1	Configuration	2	6.1	Calibration steps	14
1.2	Beam current	2	6.2	Data Streams	15
1.3	Calibration plan	3	6.3	Calibration with CW RF	15
1.4	Cross-calibration	3	6.3.1	filtering effects	15
2	Beam-cavity theory	3	6.3.2	bunch charge	16
2.1	Single isolated bunches	5	6.3.3	beam current	17
2.2	Closely spaced bunches	6	6.3.4	dark current	17
3	S-parameter theory	6	6.4	Fitting	17
4	Bench measurements	8	7	References	17
4.1	Missing power	8	8	Acknowledgements	18
4.2	Connector losses	9	1	Introduction	
5	Circuit model	10			
5.1	Uncoupled cavity	10			
5.2	2-port coupled cavity with losses	11			
5.3	Transformer ratio	11			
5.4	Series resistors	12			
5.5	S-parameters from the circuit model	12			
5.6	Fitting the model to the data	13			
5.6.1	Loss-less model	13			
5.6.2	Model with losses	14			
5.6.3	Net effect of losses	14			

*Work supported in part by the DOE Contract DE-AC02-76SF00515. This work was performed in support of the LCLS-II project at SLAC.

1 Introduction

An RF cavity, called an Average Current Monitor (ACM), is used to measure beam current. When an electron bunch passes through the cavity it leaves behind some RF energy. Some of this energy is coupled out to RF electronics which process the RF signal and generate output data in various registers. This article is about how we can accurately infer the bunch charge and beam current directly from the data in the registers, without the need to refer to beam current measurements by other devices.

In this section we discuss the basic ACM configuration, define exactly what is meant by ‘beam current’ and the plan for calibrating the system. In Section 2 we discuss the cavity voltage generated by the passage of a charge. The voltage only depends on

the frequency and the fundamental mode R_a/Q_0 factor; the R_a/Q_0 factor depends only on the cavity shape and not on the resistivity of the cavity walls. Section 3 covers the measurement, via S-parameters, of Q_0 and the parameters which determine the coupling of the cavity voltage to the attached transmission lines. If the small losses in the coupler and vacuum feedthroughs are ignored, approximate results can be obtained directly from the S-parameters at the resonant frequency. However measurements off-resonance show small but somewhat significant losses which tend to reduce the signal from the cavity. The affect of these losses is accounted for making a lumped element circuit model and adjusting the circuit parameters to fit the S-parameter data, and is discussed in Section 5. In the last section we discuss the overall calibration process and the details of how the calibration data is used.

1.1 Configuration

Figure 1 shows the cavity, loop couplers, vacuum feedthroughs and some of the transmission lines for an installed ACM. The loop couplers are made of stainless steel, as is the cavity. The connectors are standard 90 degree Type-N connectors. Ports 1 and 2 are nominally the same and provide redundant RF signals. The Test port is very weakly coupled to the cavity and is used to provide a pilot tone that is sensed through ports 1 and 2 to guarantee the integrity of the system. Low loss transmission lines called long haul cables, which can be as much as 30 m long, connect the cavity in the tunnel to electronics in the gallery outside the shielding that process the signals. The ‘calibration reference plane’, is the where the long haul cables are disconnected for calibrations measurements.

1.2 Beam current

For the purpose of protecting against thermal damage by the beam we have chosen to define ‘beam current’ to be the total charge that has passed through an ACM divided by the duration of a continuously updated integration window, ΔT . If $q_{\Delta T}$ is the total charge that passed through the ACM during the time

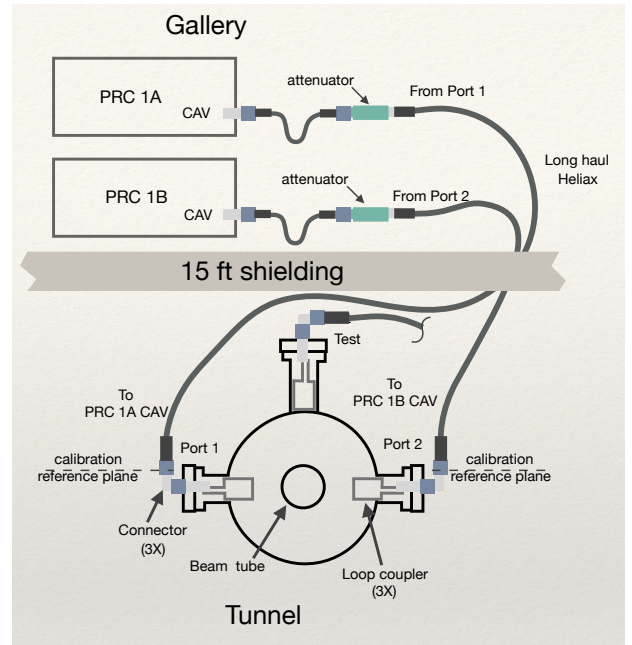


Figure 1: Schematic of an ACM cavity in the Tunnel with a standard configuration of couplers, vacuum feedthroughs, and cables to the receiver electronics in the Gallery

window, then the beam current, I , is:

$$I \equiv \frac{q\Delta T}{\Delta T}. \quad (1)$$

The total charge includes that produced by the desired photo-produced bunches as well as by any dark current that might be present. Dark current can be from two different sources. Gun dark current is emitted CW at the gun frequency of 187 MHz. Superconducting accelerating cavity dark current is also CW and is emitted at 1.3 GHz. Both have a very narrow bandwidth compared with low repetition rate photo-produced bunches.

In practice ΔT , is chosen to be about 1 millisecond and is not varied. It is long compared with the cavity field decay time. It is short compared with the time it takes for heat to diffuse significantly. Since ΔT , is well known, calibrating beam current amounts a calibrating $q\Delta T$.

1.3 Calibration plan

With simulations, given the detailed shape of the cavity, we can accurately calculate the ratio of the cavity voltage amplitude in the fundamental mode to the charge of the bunch that just produced it. To complete the calibration we only need to determine the relationship between the cavity fields and receiver register counts. This is done in two steps: measuring the cavity coupling parameters and separately measuring the relationship between the voltage emitted by the cavity and the register counts.

1.4 Cross-calibration

Three other means of measuring bunch charge are available at LCLS and can be cross-calibrated with the ACMs. Confidence in the beam charge measurement is enhanced by the extent to which these independently calibrated devices agree.

Integrated Current Transformers (ICTs) are located near the gun and about 100 m downstream of the ACMs. If we assume there is negligible loss of beam between, ICTs can be cross-calibrated with the ACMs, at least at modest repetition rates. ICTs provides a measurement of photocurrent charge, whereas

the ACM is designed to measure total beam current as defined above, but the ACMs can also measure charge provided the dark current contribution is negligible. While confidence in ICT measurements is generally good [1], the ICT installation at LCLS is new. ICT calibration is discussed in [2].

There are numerous BPMs in the copper linac which are calibrated to match a toroid that was reported to have been used in the PEP storage ring. However, no documentation for this toroid has been found, and it was moved from a storage ring and put in a low rep-rate linac. Nevertheless, this BPM calibration has been used for years at LCLS and can be compared with the ACM measurement once the SC beam reaches the copper linac BPMs.

A Faraday cup device designed to measure bunch charge or current in the 100 MeV diagnostic line with up to 60 Hz repetition rate, is located just downstream of the ACMs. If we assume there are no losses from the ACM location through the kicker and diagnostic line, then the Faraday cup may be cross-calibrated with the ACMs.

2 Beam-cavity theory

An arbitrary electromagnetic field in the cavity can be described as a superposition of normal modes [3]. The ACMs cavities were designed so that the lowest frequency mode is 1.3 GHz and is well separated from the next higher frequency mode.

Cavity voltage, V_c , is defined as the maximum voltage gain a charge could get from the fundamental mode field by passing through the cavity at the speed of light on the cavity axis. Generally V_c is a function of time. If there is no field present initially, then just after a charge passes through the cavity the cavity voltage in the fundamental mode is

$$V_q = \frac{\omega_0}{2} \frac{R_a}{Q_0} q, \quad (2)$$

where ω_0 is the fundamental mode frequency divided by 2π , (R_a/Q_0) is the shape-dependent and transit-time dependent factor for the fundamental mode, and q is the bunch charge. (See Eq. 2 of [4].) V_q is less than the instantaneous integral of the electric field

along the beam path by the transit time factor, which for the ACMs was calculated to be 0.775.¹ The bunch charge is then,

$$q = \frac{2}{\omega_0} \frac{V_q}{R_a/Q_0} . \quad (3)$$

The definition we use for the shunt impedance, R_a , in the factor R_a/Q_0 , is the so-called accelerator definition:

$$R_a \equiv \frac{V_c^2}{P_c}, \quad (4)$$

where V_c is the cavity voltage as defined above. In the case of a single bunch passage, V_c is equal to V_q just after a bunch passage and then exponentially decays in time with a field decay time constant of τ .

P_c is defined as the time varying average-over-cycle power dissipated in the cavity walls.² V_c and P_c are functions of time and can include the superposition of fields generated by multiple bunches passing through at different times.

Given a 3-dimensional representation of the cavity, its coupling loops, and the attached beam pipes, well-developed simulation tools can accurately calculate R_a/Q_0 and ω_0 . A representation of such a simulation geometry for the ACMs is shown in Figure 2 and yields value $R_a/Q_0 = 173.762 \, \Omega$. Since R_a/Q_0 does not depend on material properties, the accuracy of determining R_a/Q_0 is limited only by the accuracy of the representational geometry.

On the other hand, because we cannot measure the cavity fields directly, determining V_q is not straightforward. Our knowledge of V_q comes from measurements of power emitted from the coupling ports and a detailed understanding the coupling strength of the fundamental mode to power emitted at the Ports. In the cavity and coupler, RF loss depends on the high-frequency surface resistivity which is only approximately known; it can depend on surface finish, temperature, materials, and even the particular heat of the alloys used. Coupling strength depends on the exact geometry of the loop couplers and their

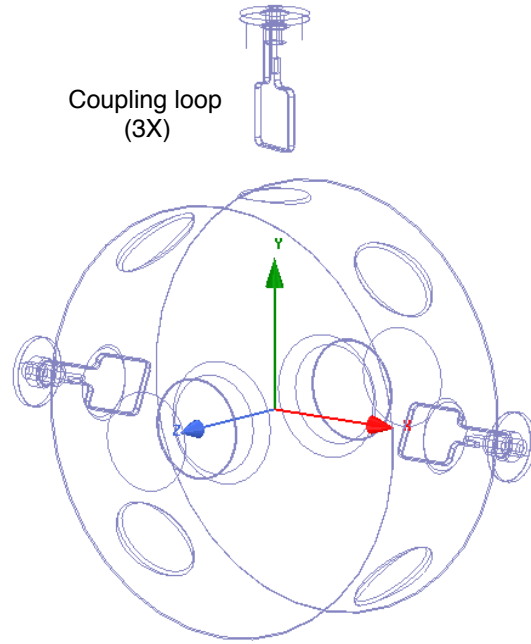


Figure 2: Wireframe of the HFSS model by Dymenso [5].

¹Personal communication: Zenghai Li

²In this note we refer to RF power terms as power averaged over a cycle (1/2 of peak-of-cycle power).

precise orientation with respect to the fundamental mode axis. To take into account the effects of these complications, we measure S-parameters and use theory described in the next Section.

2.1 Single isolated bunches

In the following discussion Port subscripts are suppressed with the understanding that the terms in the equations apply to whichever port is of interest. For example, Z_0 means Z_{01} , if applied to Port 1, and Z_{02} , if applied to Port 2. The standard definition of a port coupling parameter is:

$$\beta \equiv \frac{P_e}{P_c}. \quad (5)$$

If we define V_e as the peak-of-cycle voltage of the wave emitted from the cavity, then

$$P_e = \frac{V_e^2}{2Z_0}. \quad (6)$$

Combining Equation 4, 5, and 6 we have

$$\beta \frac{V_c^2}{R_a} = \frac{V_e^2}{2Z_0}. \quad (7)$$

For a single isolated bunch passing through the cavity, in Equation 7 we can put V_q in place of V_c , and then use Equation 3 to obtain an expression for V_e in terms of charge and other factors.

$$\frac{\beta}{R_a} \left(\frac{\omega_0 R_a}{2 Q_0} q \right)^2 = \frac{\hat{V}_e^2}{2Z_0}. \quad (8)$$

Here we introduce the symbol \hat{V}_e to denote the peak value of V_e which occurs just after a single bunch passes through. Solving for q yields,

$$q = \hat{V}_e \frac{1}{\omega_0} \sqrt{\frac{2Q_0}{\beta Z_0 (R_a/Q_0)}}, \quad (9)$$

$$(10)$$

or in terms of emitted power,

$$q = \frac{2}{\omega_0} \sqrt{\frac{\hat{P}_e Q_0}{\beta (R_a/Q_0)}}, \quad (11)$$

where \hat{P}_e is the averaged-over-cycle of the emitted power just after the bunch passed through the cavity. So if we measure, just after the bunch goes through the cavity, the peak of the emitted voltage or the average-over-cycle of the emitted power, we can determine the bunch charge.

Substituting the values determined from the bench measurements of ACM1 given in Table 3 we have:

$$q [pC] = 122.7 \hat{V}_e [V], \quad (12)$$

assuming a 50 Ω perfectly terminated transmission line is connected to the port.

We define the the running integral of the emitted voltage magnitude as,

$$\mathcal{I}(t) \equiv \int_{t-\Delta T}^t V_e(t') dt', \quad (13)$$

where the time dependence of V_e is explicitly shown. Expressed in terms of the emitted power the integral is,

$$\mathcal{I}(t) = \int_{t-\Delta T}^t \sqrt{2P_e(t') Z_0} dt'. \quad (14)$$

To a very good approximation, a single isolated bunch arriving within the integration window contributes the same amount to \mathcal{I} no matter when it arrives within the window. That is because the integration window width ΔT is more than three orders of magnitude longer than cavity field decay time, τ [4]. This implies that for a single isolated bunch,

$$\mathcal{I} \approx \hat{V}_e \tau, \quad (15)$$

for times within ΔT after the bunch arrival time, and $\mathcal{I} = 0$ for other times.³

The cavity field decay time $\tau = 2Q_L/\omega_0$, where Q_L is the 'loaded Q'. Using Eq. 36 for Q_L in Eq. 15 we have:

$$\mathcal{I} \approx \hat{V}_e \tau = \hat{V}_e \frac{2}{\omega_0} \frac{Q_0}{1 + \beta_1 + \beta_2}. \quad (16)$$

³When the bunch arrival time is near the ends of the integration window $\hat{V}_e \tau$ is a temporarily an over- or under- estimate of the contribution of that bunch to the integral.

Combining Eq. 9 and Eq. 16 yields an expression for \mathcal{I} in terms of the known quantities and bunch charge:

$$\mathcal{I} \approx \frac{q}{1 + \beta_1 + \beta_2} \sqrt{2\beta Q_0 \left(\frac{R_a}{Q_0}\right) Z_0}. \quad (17)$$

In numeric terms, given the fitted model values in Table 3:

$$\mathcal{I} [\mu V \cdot ms] \approx 2.535 q [pC]. \quad (18)$$

2.2 Closely spaced bunches

Provided beam bunches pass through the cavity at the same cavity phase, it turns out the integral of the magnitude of the cavity voltage only depends on the total charge passing through the cavity during the integration window, even if bunches are closely or unevenly spaced and the decaying field from one bunch overlaps with that of another [4].

If $q_{\Delta T}(t)$ is the total charge that passed through the cavity at time t in the past ΔT , then from Equation 17

$$\mathcal{I}(t) \approx \frac{q_{\Delta T}(t)}{1 + \beta_1 + \beta_2} \sqrt{2\beta Q_0 \left(\frac{R_a}{Q_0}\right) Z_0}. \quad (19)$$

Substituting $I(t) = q_{\Delta T}(t)/\Delta T$ into Eq. 19 and setting it equal to Eq. 14 and solving for $I(t)$ yields

$$I(t) = \frac{1 + \beta_1 + \beta_2}{\sqrt{\beta Q_0}} \int_{t-\Delta T}^t \sqrt{\frac{P_e(t')}{R_a/Q_0}} \frac{dt'}{\Delta T}. \quad (20)$$

This equation relates the beam current and the emitted power. The characteristic line Z_0 does not appear in this last expression.

3 S-parameter theory

In this section we derive the theoretical relationship between S-parameters for Port 1 and Port 2, and the cavity parameters β_1 , β_2 , Q_L , and Q_0 . Knowledge of these cavity parameters is needed in order to relate what we can measure — the power emitted from the cavity — to voltage in the cavity, which we need to know to determine the charge.

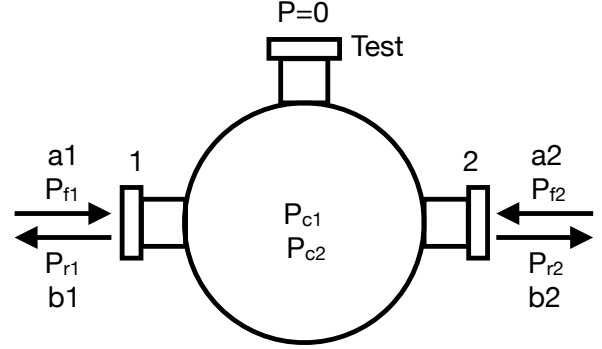


Figure 3: Schematic of power flows during network analyzer tests and ‘power wave’ coefficients

By design the two Probe ports have strong coupling to the fundamental cavity mode, while the coupling of the Test port to either Probe port is so weak its effect can be ignored in determining the bunch charge from measured RF. The two Probe ports are nominally identical but are expected to have some small differences in coupling strengths and therefore produce somewhat different RF signals for the same bunch charge.

Figure 3 schematically shows the power flows at the ACM cavity ports. When connected the NA alternately switches between putting power into port 1 while providing a matched load on port 2, and the reverse: putting power into port 2 while providing a matched load on port. For each configuration the NA measures the ‘power wave’ coefficients ‘a’ and ‘b’ that describe the amplitude of the voltage wave going toward (forward), or away from (reverse), the ACM. We define:

P_{f1} is the power flowing from port 1 of the NA into port 1 of the ACM.

P_{f2} is the power flowing from port 2 of NA into port 2 of the ACM.

P_{r1} is the power flowing from the ACM port 1 into the NA port 1.

P_{r2} is the power flowing from the ACM port 2 to the NA port 2.

P_{c1} is the power dissipated in the walls of the ACM when the NA is sending power to port 1.

P_{c2} is the power dissipated in the walls of the ACM when the NA is sending power to port 2.

These six values change depending on whether the NA is sending power to port 1 or to port 2. In particular the power dissipated in the cavity will be change if the coupling strengths of the two ports differ even if the incident power from the NA is the same.

The coupling strengths β_1 and β_2 are defined as the ratio of power emitted, or radiated, from a port to the power dissipated in the cavity walls. The power ‘emitted’ or ‘radiated’ refers to the power flowing from a port due solely to the field in the cavity and does not include power reflected from the port. When the NA is sending power to port 1 all power coming out of port 2 is radiated power — there are no reflections from port 2. In that case

$$\beta_2 = P_{r2}/P_{c1} \quad (21)$$

Similarly when the NA is sending power to port 2 all power coming out of port 1 is the radiated power, and

$$\beta_1 = P_{r1}/P_{c2}. \quad (22)$$

First consider the case where the NA applies power to port 1 only and puts a matched load on port 2. Results for the case where the NA applies power only to port 2 can be obtained from this case by interchanging the indices. Conservation of energy implies:

$$P_{f1} = P_{c1} + P_{r1} + P_{r2} \quad (23)$$

Solving for P_{c1} and substituting in eq. 21 gives,

$$\beta_2 = \frac{P_{r2}}{P_{f1} - P_{r1} - P_{r2}} \quad (24)$$

The S parameters are defined as:

$$S_{11} = \left. \frac{b_1}{a_1} \right|_{a_2=0} \quad (25)$$

$$S_{22} = \left. \frac{b_2}{a_2} \right|_{a_1=0} \quad (26)$$

$$S_{21} = \left. \frac{b_2}{a_1} \right|_{a_2=0} \quad (27)$$

$$S_{12} = \left. \frac{b_1}{a_2} \right|_{a_1=0} \quad (28)$$

where a ’s and b ’s are the power wave coefficient [6] — similar to forward and reverse traveling wave amplitudes. In terms of the power flows:

$$|S_{11}|^2 = \left. \frac{P_{r1}}{P_{f1}} \right|_{P_{f2}=0} \quad (29)$$

$$|S_{22}|^2 = \left. \frac{P_{r2}}{P_{f2}} \right|_{P_{f1}=0} \quad (30)$$

$$|S_{21}|^2 = \left. \frac{P_{r2}}{P_{f1}} \right|_{P_{f2}=0} \quad (31)$$

$$|S_{12}|^2 = \left. \frac{P_{r1}}{P_{f2}} \right|_{P_{f1}=0} \quad (32)$$

By dividing numerator and denominator of equation 24 by the forward power into port 1, P_{f1} , we get

$$\beta_2 = \frac{P_{r2}/P_{f1}}{1 - P_{r1}/P_{f1} - P_{r2}/P_{f1}} \quad (33)$$

which can be written in terms of the S-parameters as

$$\beta_2 = \frac{|S_{21}|^2}{1 - |S_{11}|^2 - |S_{21}|^2}. \quad (34)$$

By interchanging indices we can write the expression for β_1

$$\beta_1 = \frac{|S_{12}|^2}{1 - |S_{22}|^2 - |S_{12}|^2}. \quad (35)$$

These equations for coupling strengths agree with those in [7], equation 170.

If the loaded Q, Q_L , is measured the β ’s can be used to calculate Q_0 via,

$$Q_0 = Q_L(1 + \beta_1 + \beta_2). \quad (36)$$

For example, see [8] p. 148.

4 Bench measurements

In this section we describe room temperature bench measurements of the first unit, ACM1. The measurements show that there are some small but significant losses not accounted for in the theory described in Section 3 due to additional elements used to connect the NA to the cavity, and the resistivity of the coupling loops.

The measurements were taken with the NA attached to the cavity as shown in Figure 4. A 50 Ω termination is put on the Test port, although it has essentially no effect because the Test port coupling is so weak. An RF elbow is connected to each of the Port 1 and Port 2 vacuum feedthrough connectors and left in place to help protect the fragile vacuum feedthroughs. The NA cables are connected to the elbows.

Before attaching the NA to the ACM the NA is calibrated with an electronic calibration unit using the same cables that are to be connected to the ACM. Electronic calibration has the effect of applying frequency dependent offsets to the forward and reflected power measurements such that, ideally, if the cables from the two ports of the NA were connected together with a perfectly matched, lossless, barrel connector, measurement of both $|S_{11}|^2$ and $|S_{22}|^2$ would be exactly 1 over the frequency range of the calibrations. Electronic calibration takes does not take into account effects due to RF elbows.

Measurements for ACM1 are shown in Figure 5, and the resulting calculated RF parameters are shown in Table 1. The values for β_1 and β_2 are computed from the S-parameters exactly at resonance via Eqs. 34 and 35. The loaded Q is computed from the half-maximum points of the transmitted power ([3] p. 489) which is proportional to $|S_{21}|^2$. Q_0 is then calculated using Eq. 36.

4.1 Missing power

Measurements over an extended frequency range are shown in Figure 6. The transmitted power fraction is $|S_{21}|^2$, and reflected power fraction is $|S_{11}|^2$. These data demonstrate that there are some losses that are not accounted for cavity wall losses alone. This

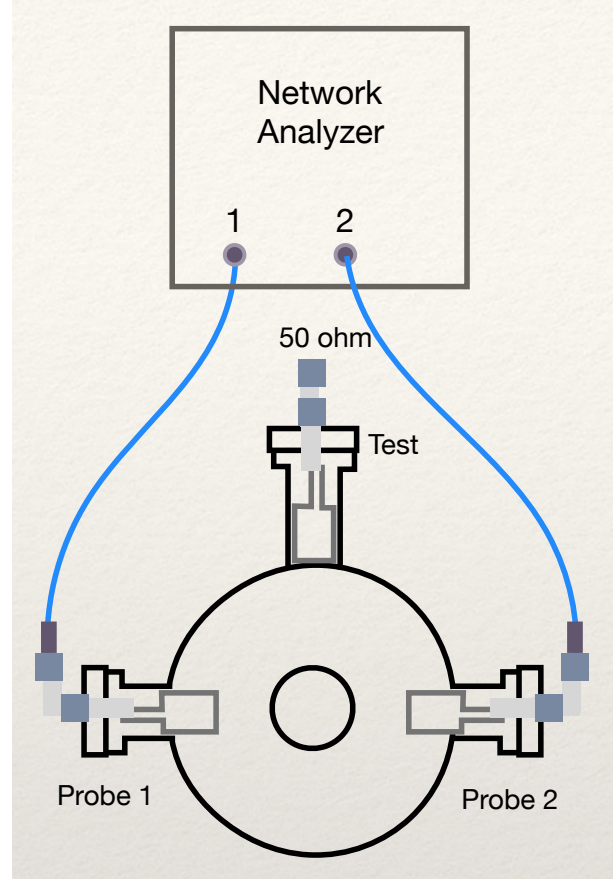


Figure 4: NA and ACM configuration for S-parameter measurements.

Table 1: Nominal RF parameters calculated directly from S-parameter measurements using formulae in Section 3.

β_1	0.647
β_2	0.663
Q_L	1265
Q_0	2922

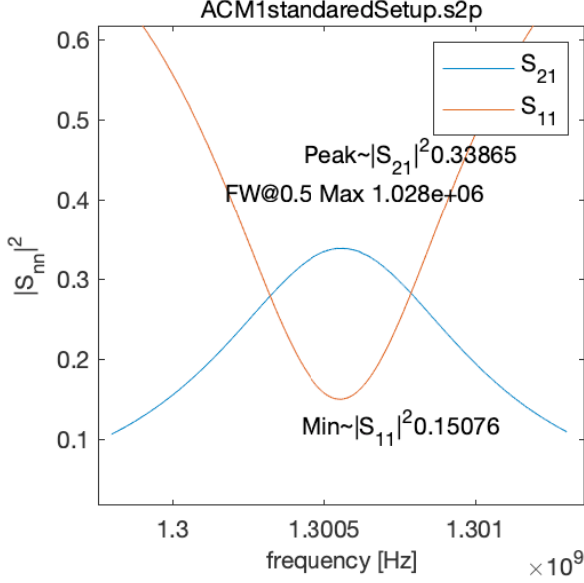


Figure 5: Selected S-parameters measurements of ACM1.

is clear in the off-resonance part of the data where transmitted power is completely negligible yet the reflected power fraction is only 91.4% (not 100%). Because the coupling betas are of order 1, the power transmitted out of port 2 must be comparable to the power dissipated in the cavity walls, so we can conclude that, well away from the resonance, the power dissipated in the cavity walls is also negligible. The curve labeled ‘Lost’ represents the difference between 1 and the sum of reflected and transmitted fractions. Off resonance, the Lost fraction is about 8.6% of the total power.

What happens to this missing power, and how do these losses affect the determination of the beam current? If the actual losses are greater than those in the theory, then the measured RF signal will be weaker than predicted, we would underestimate V_q and the beam current would be underestimated.

Lacking any other candidates, we presume the missing power is due to losses in the elbows and vacuum feedthroughs. Elbows are expected to cause a power loss of 1.5% per pass, based on measurements

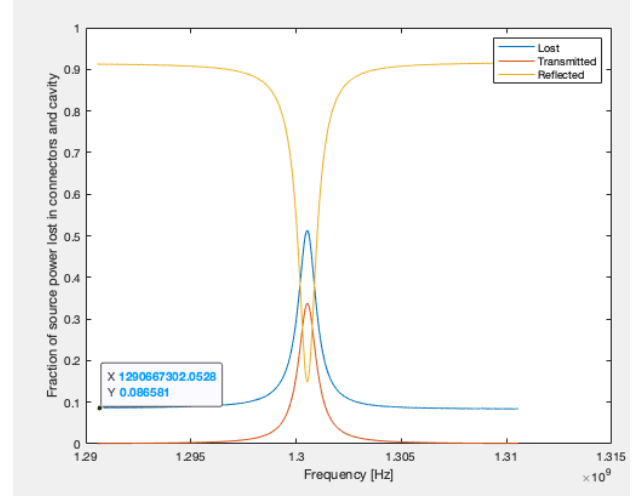


Figure 6: Measured normalized power as a function of frequency for ACM1.

shown in Section 4.2. Off-resonance, the reflected power must pass through the elbow twice, so the net loss of power is 3%. The vacuum feedthroughs are custom made ceramic-brazed feedthroughs designed to accommodate a Type-N connector. Losses can occur at the contact points and on center conductor, which is believed to be made of Kovar. Because coupling loops are well coupled to the cavity field and the cavity field is negligible when driven off-resonance, they should not contribute to the missing power.

When the cavity is driven on-resonance we presume that elbow and feedthrough losses are the same as they are when driven off-resonance. Consequently the measured S-parameters don’t exactly reflect the power entering or leaving the cavity, where the ‘cavity’ is thought of as the ideal cavity modeled in the simulation and includes stainless steel coupler loops terminated with 50 ohms.

4.2 Connector losses

NA measurements were made to determine the losses one might expect at 1.3 GHz from the 90 degree elbow connectors that connect the transmission lines to the ACM cavity. The setup for the connector measure-

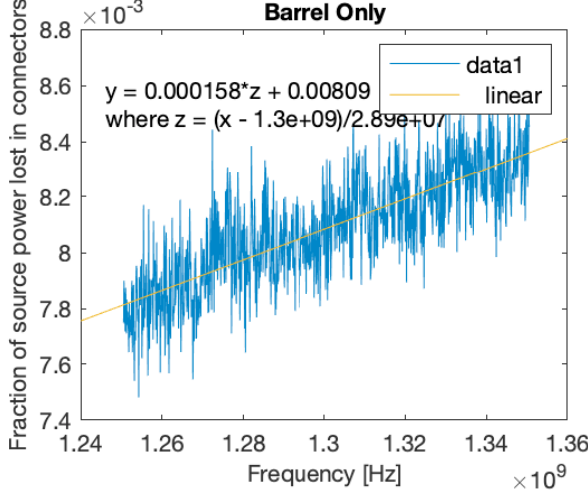


Figure 7: Fractional power lost in a Barrel connection.

Table 2: Barrel and 90 degree elbow fractional power losses

Barrel loss	=	0.00809
Barrel + 2 elbows	=	0.03828
Loss per elbow	=	0.0151

ment was to first connect the calibrated NA across a series combination of 90 degree elbow - barrel - 90 degree elbow, and measure the lost power fraction. The fraction of absorbed power is assumed to be power that is neither reflected nor transmitted and is equal is:

$$P_{abs} = 1 - |S_{11}|^2 - |S_{21}|^2$$

We also measured the lost power with just the barrel present. The data are shown in Figure 7 and 8. The loss from the connectors was within manufacturers specifications and is summarized in Table 2. The fractional power loss from two elbows in series is about 3%.

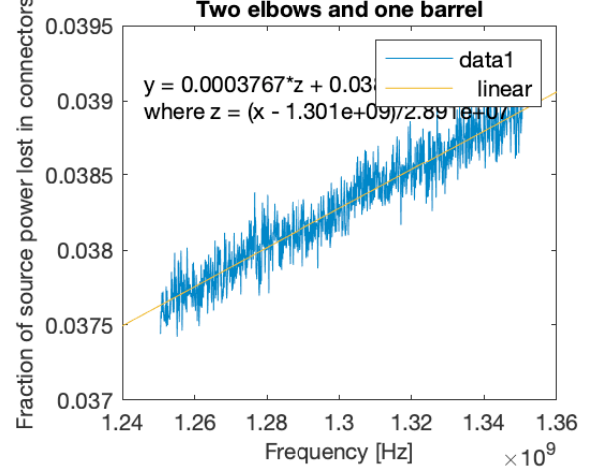


Figure 8: Fractional power lost in the Elbow-Barrel-Elbow connection.

5 Circuit model

To address the small but significant losses of elbow and vacuum feedthrough, we construct a lumped-element circuit model of the ACM which includes small-value series resistors to represent these losses. We find the best values for the circuit model elements by varying their values and comparing model predictions S-parameters with those obtained from bench tests. From this optimized circuit model we can extract a more accurate value for ratio of power emitted by the cavity to beam charge passing through the cavity.

5.1 Uncoupled cavity

The impedance of an isolated RF cavity is typically modeled as a RLC circuit as shown in Figure 9. See for example [8] and [3]. In this basic model, values for the lumped elements are chosen as

$$R = \frac{R_a}{2} \quad (37)$$

$$L = \frac{R_a/Q_0}{2\omega_0} \quad (38)$$

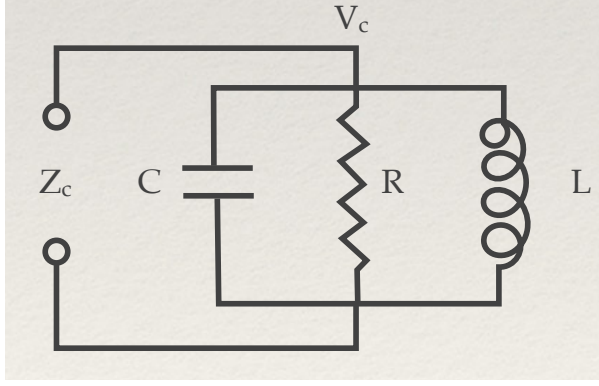


Figure 9: Lumped element circuit model of an isolated ACM cavity.

$$C = \frac{2}{(R_a/Q_0)\omega_0}. \quad (39)$$

The impedance of the isolated cavity, Z_c , can be determined from

$$\frac{1}{Z_c} = j\omega C + \frac{1}{R} + \frac{1}{j\omega L}.$$

5.2 2-port coupled cavity with losses

The circuit model representing a bench test configuration is shown in Figure 10 with transmission lines and NA source impedances explicitly shown. It is the same type model a cavity coupled to a transmission line used by [8] and [3], but it has two ports which include additional series resistors, ΔR_1 and ΔR_2 , to take into account losses in the feedthroughs and elbows. Coupling to the external ports is modeled as a transformer with turns ratio n_1 (or n_2 for port 2) in series with a resistor needed to account for the missing power. This model allows for coupling strength and losses to be different at the two ports. The model allows for unequal impedance of the transmission lines connected from the ACM ports to the NA ports, though such differences are expected to be negligible.

5.3 Transformer ratio

The choice of transformer ratio, n , needs some discussion, because it depends on the exact definition of the coupling parameter β . The standard definition for the coupling parameter β is the ratio of power emitted from the cavity, P_e , to the power dissipated in the cavity walls, P_c :

$$\beta = \frac{P_e}{P_c}. \quad (40)$$

P_e , just like P_c , is defined as the time varying average over cycle of the power emitted from the port.

Since we decided to keep an elbow connector attached to the ACM feedthrough more or less permanently, so that we do not fatigue the vacuum feedthrough pins of the coupling ports, we choose the definition of ‘power emitted’ to refer to the power that is emitted after losses in the elbow and vacuum feedthrough. This remaining power is the power that goes toward the NA on the calibrated transmission line.

Furthermore, we are only interested in the power associated with the fundamental resonance of the cavity for which we know the R_a/Q_0 from simulation. Such power follows the resonant line shape of the fundamental mode.

Referring to symbols in the circuit model in Figure 10, power emitted from Port 1 is

$$P_{e1} = \frac{V'^2}{Z_{01} + \Delta R_1}.$$

Here we can see that effect of the series resistor is to reduce the emitted power. Since $V'_1 = V_c/n_1$, we have

$$P_{e1} = \frac{V_c^2}{n_1^2(Z_{01} + \Delta R_1)}. \quad (41)$$

Substituting $P_c = V_c^2/R$ and P_{e1} from Eq. 41 in Eq. 40 leads to

$$n_1 = \sqrt{\frac{R}{(\Delta R_1 + Z_{01})\beta_1}}. \quad (42)$$

An expression for the transformer ratio for Port 2 can be obtained by exchanging 1 and 2 in the subscripts.

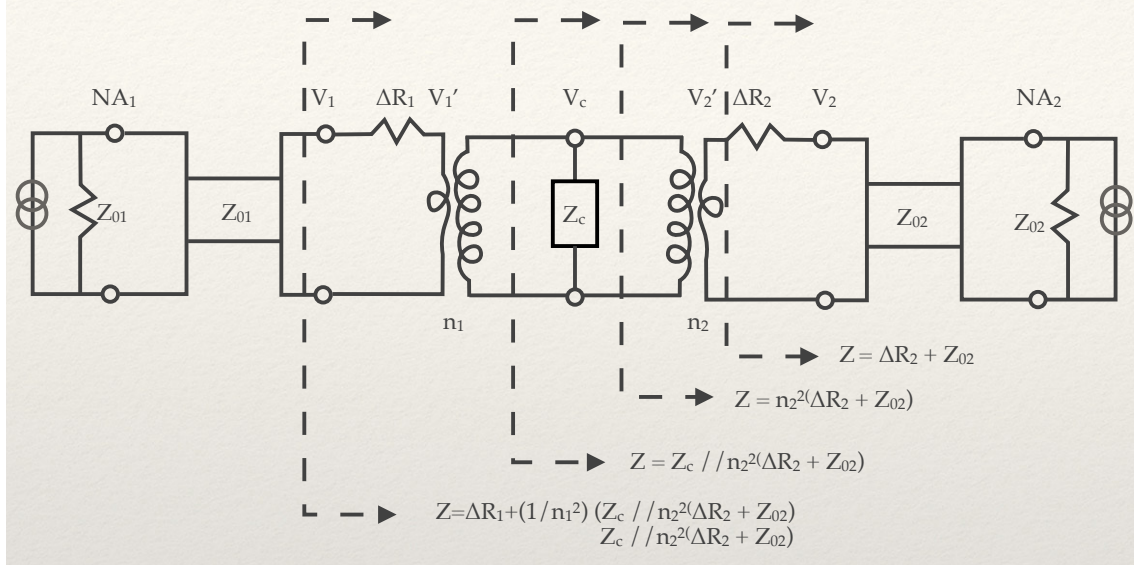


Figure 10: Circuit model of an ACM under bench test .

5.4 Series resistors

Well off-resonance the cavity acts as short circuit — high frequencies are shorted by the capacitance, and low frequencies are shorted by the inductance. Looking from the NA Port 1 toward the cavity, we would see a short in series with the resistor. We can calculate the value of the resistor from the reflection coefficient for Port 1, Γ_1

$$\Delta R_1 = Z_{01} \frac{1 + \Gamma_1}{1 - \Gamma_1} \quad (43)$$

For the ACM1 data shown Section 4.1 the off-resonance reflected power fraction is 0.913. That corresponds to an off-resonance reflection coefficient of $\Gamma_1 = \sqrt{0.913} = 0.956$. With Z_{01} of 50 ohms, Equation 43 yields $\Delta R_1 = 1.13$ ohms.

5.5 S-parameters from the circuit model

The magnitude of the model S-parameters can be calculated as a function of frequency and compared with measurements. The approach is to start by calculating impedances sequentially as shown in Figure 10. In

the figure, the symbol ‘//’ means that the impedance is formed by a parallel combination of the terms on either side of it. Start at the rightmost section line, the impedance seen looking at the circuit to the right is a series combination of ΔR_2 and the line impedance Z_{02} . On the other side of Port 2 this impedance is transformed by a factor of n_2^2 . At the next section line we see a parallel combination of the transformed impedance and the bare cavity impedance Z_c . At the leftmost section line we see the previous impedance transformed by the $1/n_1^2$. That final impedance is what the NA sees.

With the impedance seen by the NA calculated, we can calculate the reflection coefficient and the $|S_{11}|$. We also can calculate the voltage at the cavity assuming an arbitrary voltage wave amplitude generated at the NA heading toward the cavity. From the cavity voltage is possible calculate the magnitude of outgoing wave from Port 2 and $|S_{21}|$. The notation was chosen so that other S-parameters are obtained by interchange the 1 and 2 subscripts.

A voltage wave with amplitude V_+ on the transmission line from the NA traveling toward ACM port 1

sees a reflection coefficient:

$$\Gamma_1 = \frac{Z_1/Z_{01} - 1}{Z_1/Z_{01} + 1} \quad (44)$$

where Z_1 is the impedance of the circuit looking toward the right in the diagram at the leftmost section line in Figure 10.

The cavity voltage can be calculated in terms of the power going toward the ACM, $P_{f1} = V_+^2/Z_{01}$, and circuit parameters as follows:

$$V_c = n_1 V_1' \quad (45)$$

$$V_1' = V_1 \frac{Z_1 - \Delta R}{Z_1} \quad (46)$$

$$V_1 = V_+ + V_- = V_+(1 + \Gamma_1) \quad (47)$$

$$V_c = n_1 \sqrt{P_{f1} Z_{01}} (1 + \Gamma_1) \frac{Z_1 - \Delta R}{Z_1}. \quad (48)$$

The voltage generated on the Port 2 transmission line can now be calculated. We have

$$V_2 = \frac{V_c}{n_2} \frac{Z_{02}}{\Delta R_2 + Z_{02}}, \quad (49)$$

assuming there is no incoming wave to ACM Port 2 when the NA Port 1 is generating power. The magnitude of the S-parameters are then calculated from the ratio of magnitude in voltage waves:

$$|S_{21}| = \sqrt{\frac{V_2}{V_+}} \quad (50)$$

$$|S_{11}| = |\Gamma_1| \quad (51)$$

The other S-parameters are obtained by interchanging $1 \leftrightarrow 2$.

5.6 Fitting the model to the data

The objective is to find the values of β_1 , β_2 , ΔR_1 , ΔR_2 and Q_0 for which predictions from the circuit model match the S-parameter measurements. As usual we assume that in performing the measurements the NA and the transmission lines are calibrated for a nominally 50 Ω characteristic line impedance which is not varied in the fitting.

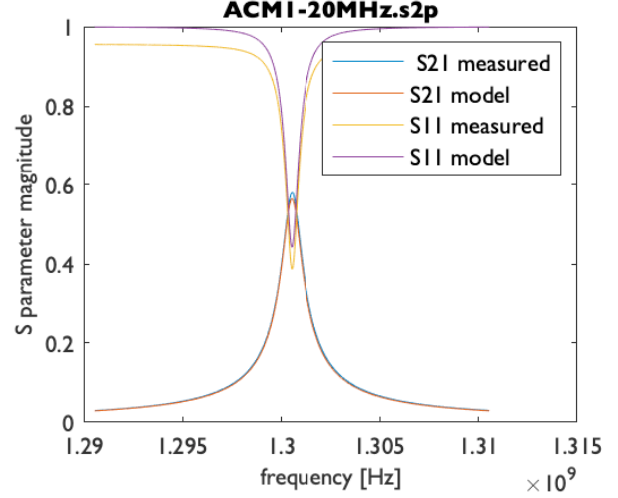


Figure 11: Prediction using the loss-less model compared with measured S-parameters.

5.6.1 Loss-less model

It is instructive to first look at the predictions for β_1 , β_2 , and Q_0 , derived from S-parameter measurements on-resonance using the method in Section 3, which assumes no losses in the elbows and feedthroughs. If these values are then used to derive the values for the elements in the circuit model, the circuit model can then predict the S-parameter response at all frequencies, not just on-resonance. This prediction is shown plotted as a function of frequency together with measured S-parameters in Figure 11. An almost identical set of curves can be obtained for the S-parameters with the 1 and 2 indices exchanged and is not shown.

Clearly the loss-less version of the circuit model does not completely reproduce the measurements. Most notable is the vertical offset in the S_{11} prediction with respect to the measured data is apparent at all frequencies. A small underestimate of the S_{21} prediction is also evident.

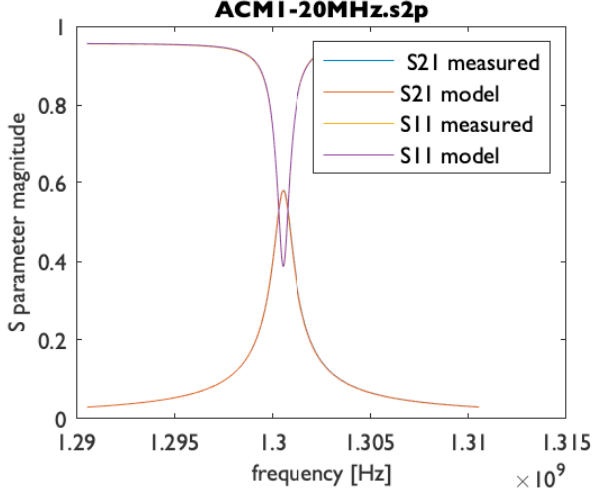


Figure 12: Prediction using the Modified model compared with the magnitude of the measured S-parameters. Predicted and measured curves lay on top of one another.

5.6.2 Model with losses

Using a version of the circuit model which includes losses in the coupler and vacuum feedthroughs, impedances and reflection coefficients were calculated and the magnitude of the S-parameters were derived. In this model only β_1 , β_2 , ΔR_1 , ΔR_2 and the resonant frequency were adjusted. The fitted model predictions are shown plotted as a function of frequency together with the magnitude of the measured S-parameters in Figure 12. An almost identical set of curves can be obtained for the S-parameters with the 1 and 2 indices exchanged and is not shown.

The modified model essentially fits the data so well that plotted curves are indistinguishable. The sensitivity of the fit to parameters is reasonably high. For example, the fit was sensitive changes in the values of the coupling parameters β_1 and β_2 of less than 0.001. The best fit values for the fitted parameters are shown in Table 3.

Table 3: Best fit values of RF parameters for ACM1 based on bench measurements at room temperature.

β_1	0.716
β_2	0.742
Q_0	3122
ΔR_1	1.10 Ω
ΔR_2	0.97 Ω

5.6.3 Net effect of losses

Using the measurements from Dymenso [9] instead of the fitted values, we would have 2.586 as the coefficient in front of the charge — a difference of 2%. Calculated without regard to the losses in the couplers and feedthroughs the coefficient would be 2.482 — a difference of 2% in the other direction.

6 Calibration functions

The firmware and electronics of the ACM system compare a threshold value to the running sum of data points are proportional the magnitude of the emitted voltage. If the sum exceeds the threshold a fault is issued and the beams are shut down. To assign a threshold in terms of beam current we need to determine the relationship between the beam current and the running sum generated by the ACM system. This relationship we call the beam current calibration function. Similar functions are needed to relate the bunch charge and dark current to data generated by the ACM system.

6.1 Calibration steps

The calibration functions can be obtained by executing the following steps:

1. Measure the cavity RF properties by making S-parameter measurements directly on the cavity. S-parameter measurements and RF circuit analysis account for coupling strengths, vacuum feedthrough losses and cavities parameters. These measurements are described in Section 4.

2. Measure the response of the cabling and electronics using a calibrated CW RF power source in place of the cavity. This step is discussed in Section 6.3.
3. Determine the effects of filtering in the receivers from a circuit and signal processing model. This is discussed in Section 6.3.1.
4. Apply the theoretical formulae relating cavity voltage to beam charge and current. See Sections 6.3.2-6.3.4.

A detailed procedure to execute steps 1 and 2 is given in [10].

6.2 Data Streams

The three data streams that are most relevant to calibration are labeled with the symbols:

- $N \leftrightarrow$ ‘Bunch charge’: 22-bit signal proportional to the magnitude of the cavity voltage .
- $N_{int} \leftrightarrow$ ‘Beam current’: 31-bit running integral of N . This number is compared with the trip threshold.
- $N_{dark} \leftrightarrow$ ‘Dark current’: 26-bit narrowly filtered signal proportional to the magnitude of cavity voltage at 1.3 GHz.

The ‘Bunch charge’ and ‘Beam current’ data are digitized at the rate of 31.4 MHz and available as waveforms records of 32,768 points (about 4% longer than the integration window). The waveforms are sent to an IOC upon any of three triggers: fault, level-trigger, or external trigger. Many signal processing details can be found in Reference [11].

The beam current data, N_{int} , is derived directly from the same source as that used for bunch charge data by continuously summing over that last 31,488 points. The total beam current, consisting of both normal and dark current, can be inferred from this sum.

The dark current data, N_{dark} , is derived from the signal from a very narrow band filter on the down-mixed cavity voltage. It will include contributions

from dark current, as well from CW photocurrent when the repetition rate is comparable or greater than the filter bandwidth.

In theory bunch charge can be derived from the peak of the induced cavity voltage when a single isolated bunch passes through the cavity. In practice the overall peak of the bunch charge waveform, which may include the signals from multiple bunches, is used to determine charge. Since charge may vary from bunch to bunch, the charge measured in this way may be slightly higher than the average charge, particularly if the variability of charge from bunch to bunch is high.

When there are closely spaced bunches (dark current) such that the field induced by one bunch adds to the field induced by the previous bunch, the bunch charge cannot be calculated from the cavity voltage signal unless the repetition rate is known.

Photocurrent bunches are usually spaced widely enough that there is no significant overlap with the previous bunches induced field. However there is a slight field overlap, about 5%, at the highest repetition rate, ≈ 1 MHz, causing a small overestimate of the bunch charge at the highest rate.

6.3 Calibration with CW RF

Calibrating with CW RF amounts to putting a known CW signal at the cavity in place of the beam generated one and recording the counts on the data streams. A CW RF power source is desirable because CW RF power can be generated and measured with very good accuracy.

6.3.1 filtering effects

In order to apply the CW calibration to the actual sharply peak bunch signals, the effects of filtering by the circuit and signal processing must be determined and taken into account.

When a bunch goes through the cavity the cavity voltage is excited to the peak value in a few nanoseconds and subsequently decays with about a $0.5 \mu s$ time constant. The voltage signal from the cavity passes through the relatively broad-band long haul cables where it is attenuated before it reaches the

receivers. The receivers contain analog and digital electronics that filter out high frequencies and convert the signal to digital values that are proportional to the magnitude of the voltage received. Details of the receiver and signal processing design may be found in [12].

A detailed matlab model of the receiver processing was made to determine the effects of filtering. In the receiver the raw 1.3 GHz signal is attenuated, passed through a 1.4 GHz low pass filter, and mixed with 1320 MHz signal to make a 20 MHz IF signal. The IF signal is passed through another low-pass filter and through a final custom low pass filter. Then the signal is digitized at 94.1 MHz, converted to I and Q values to extract the voltage magnitude and phase, boxcar filtered, and finally decimated by a factor of three. The modeling includes all of these steps.

Results from the modeling lead to the conclusions that processing both:

- has a negligible affect on the integrated signals (i.e. beam current measurements), and
- reduces the height of the single isolated bunch signal to about 74% of the ideal.

An example of the results is shown in Figure 13, where an ideal pulse was simulated, and plotted as ‘Theory’. It has very sharp rise time. When that pulse is put through the processing model the result is the smoother, flatter curve labeled ‘Modeled’. Actual measured data points labeled ‘Measured’ are plotted as well. Only a single overall scale factor was applied to get the data to fit the modeled data. The modeled curve peak has been reduced from the original ideal curve by a ‘filter factor’

$$F_q = 0.73985.$$

This peak value of the pulse is used for the charge measurement. If calibration did not take into account this filtering effect, the reported charge would be only about 74% of the true charge.

The integral of the digitized signal over 1 ms is used for the current measurement. As noted in the figure text, the ratio of the integral of the modeled filtered, signal to the integral of the ideal signal is 1.0065. Evidently current calibration is not significantly affected by filtering.

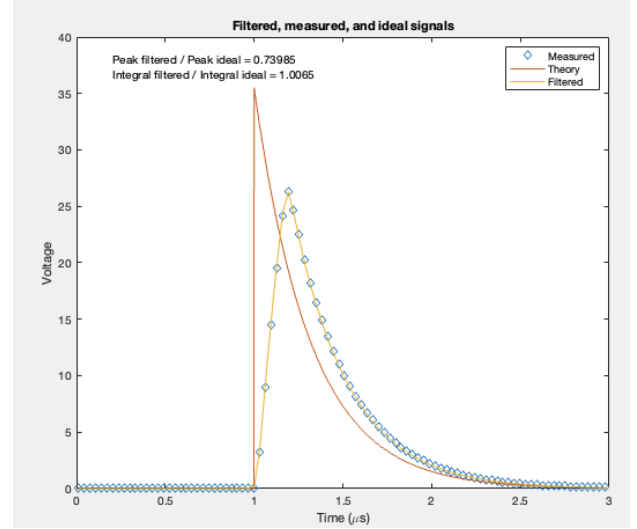


Figure 13: Effect of filtering on the calibration of the bunch charge.

6.3.2 bunch charge

P_{cal} is defined as the CW power input to the long haul cables used in place of the beam generated signal from the cavity. We can relate P_{cal} to the *peak* power emitted by a single charge q using equation 11, which relates q to \hat{P}_e . Since \hat{P}_e is the RF power emitted just after the bunch goes through, and both P_{cal} and \hat{P}_e are average-over-cycle quantities, we simply replace \hat{P}_e with P_{cal} . At the cavity side of the long haul cables, a CW signal of power P_{cal} would have the the same value as the power emitted just after the passage of bunch of charge q_{cal} .

Because of filtering the peak voltage (or square root of the power) is reduced by a factor F from the theoretical, see Section 6.3.1. In this case the relationship between calibrated charge and calibrated CW RF power is:

$$q_{cal} = \frac{1}{F_q} \frac{2}{\omega_0} \sqrt{\frac{P_{cal} Q_0}{\beta(R_a/Q_0)}}, \quad (52)$$

$$P_{cal} = F_q^2 q_{cal}^2 \left(\frac{\omega_0}{2}\right)^2 \frac{\beta(R_a/Q_0)}{Q_0}. \quad (53)$$

6.3.3 beam current

To get the relation between the calibrated current I_{cal} and P_{cal} we use Equation 20. Equation 20 is derived assuming the emitted power P_e is generated by an arbitrary set of beam bunches, including the case where a steady state cavity field is built up by closely spaced bunches. So P_{cal} can represent the beam emitted power for such a steady state case in Equation 20. Since P_{cal} is constant Equation 20 integrates to,

$$I_{cal} = \frac{1 + \beta_1 + \beta_2}{\sqrt{\beta Q_0}} \sqrt{\frac{P_{cal}}{R_a/Q_0}}, \quad (54)$$

$$P_{cal} = I_{cal}^2 \frac{(R_a/Q_0)(\beta Q_0)}{(1 + \beta_1 + \beta_2)^2}. \quad (55)$$

I_{cal} does not depend on the integration window ΔT since P_{cal} is CW and constant. A CW beam current of I_{cal} would produce an emitted CW power of P_{cal} in Eq. 55.

6.3.4 dark current

The calibration equation for dark current is the same as for (total) beam current. A dark current, I_{dark} , will generate a CW voltage on the cable with the same integrated magnitude as would be produced by a normal photo-current of the same average current. Unlike the signal processing for total beam current, the dark current signal goes through a very narrow filter (~ 1 Hz) and as a result has a lower noise floor.

6.4 Fitting

When the calibration data has been obtained for a discreet set of calibrated CW power levels, the calibration functions can be constructed.

1. Plot $I_{cal}(P_{cal})$ versus $\bar{N}_{int}(P_{cal})$ and choose a function, $I_m(\bar{N}_{int})$, that fits the data.
2. Plot $q_{cal}(P_{cal})$ versus $\bar{N}(P_{cal})$ and choose a function $q_m(\bar{N})$ that fits the data.
3. Plot $D_m = I_m(P_{cal})$ versus $\bar{N}_{dark}(P_{cal})$ and choose a fitting function $D(\bar{N}_{dark})$.

I_m , q_m , and D_m are then the measured values of beam current, bunch charge, and dark current respectively.

Because the power data is over many orders of magnitude, linear functions do not fit the data well, especially at the lower currents or charges. Since noise levels are low, a linear interpolation function works well over the whole range of measurements.

7 References

- [1] J. Bergoz, “Integrating current transformer (ICT) pulse charge accuracy,” ICT Technical Note 06.1, Bergoz Instrumentation, Espace Al-london Ouest 01630 Saint Genis Pouilly, France, July 2006.
- [2] F. Stulle and J. Bergoz, “Turbo-ICT picocoulomb calibration to percent-level accuracy,” in *Proceedings of FEL2015*, pp. 118–121, 2015.
- [3] J. Slater, “Microwave electronics,” *Reviews of Modern Physics*, vol. 18, pp. 441–512, 1946.
- [4] J. Welch, “Average current monitor beam generated signals,” Tech Note LCLS-II-TN-19-01, SLAC, 2019.
- [5] P. Borchard, “Average current monitor (ACM) sensor final design review.” Talk given at the Final Design Review for the ACM sensor, SLAC, Menlo Park, Ca, July 2019.
- [6] R. W. Anderson, “S-parameter design for faster, more accurate network design,” Hewlett Packard, Test and Measurement Application Note 95-1, Hewlett Packard, 1967.
- [7] J. Holzbauer, “RF theory and design - notes,” USPAS, 2012.
- [8] H. Padamsee, J. Knobloch, and T. Hays, *RF Superconductivity for Accelerators*. Wiley Series in Beam Physics and Accelerator Technology, John Wiley & Sons, Inc., 1998.
- [9] P. Borchard, “ACM factory acceptance test data.” Measurements by Dymenso on SN 1, September 2019.

- [10] J. Welch, “ACM Beam-RF calibration procedure,” Work Plan and Procedure LCLSII-2.4-PP-2038-R0, SLAC, 2021.
- [11] T. Allison, “LCLS-II BCS Average Current Monitor Receiver Firmware Requirements,” Safety Systems Document CD-SS-BCS-07-11-05, Rev 3, SLAC, November 2019.
- [12] T. Allison, “LCLS-II Beam Containment System Average Current Monitors ESD,” Engineering Specifications Document LCLSII-2.4-ES-1365-R0, SLAC, February 2019.

8 Acknowledgements

Christopher Nantista suggested looking off-resonance for losses which prompted the development of the circuit model. John Sikora helped extensively with measurements and supplied general RF expertise. Zenghai Li provided detailed explanations of modeling the couplers and the R/Q. Trent Allison provided data structures and power levels and very thoughtful comments. Philipp Borchard at Dymenso provided precisely tuned cavities and a set of bench measurements.